Polymer Chemistry

Thermoresponsive Polymer Brush Photocatalytic Substrates for Wastewater Remediation

Journal:	*Polymer Chemistry*
Manuscript ID	PY-COM-03-2023-000248.R1
Article Type:	Communication
Date Submitted by the Author:	03-May-2023
Complete List of Authors:	Bell, Kirsten; The Pennsylvania State University, Chemical Engineering Guo, Yiwen; The Pennsylvania State University, Chemical Engineering Barker, Samuel; The Pennsylvania State University, Chemical Engineering Kim, Seong; Pennsylvania State University Pester, Christian; The Pennsylvania State University, Chemical Engineering

COMMUNICATION

Thermoresponsive Polymer Brush Photocatalytic Substrates for Wastewater Remediation

Received 00th January 20xx,
Accepted 00th January 20xx

DOI: 10.1039/x0xx00000x

Kirsten Bell,[a] Yiwen Guo,[a] Samuel Barker,[a] Seong H. Kim,[a,b,c] Christian W. Pester*[,a,b,c]

Synthesis and characterization of a multi-responsive micron-scale heterogeneous catalyst are described. The temperature-responsive monomer *N*-isopropylacrylamide (NIPAAm) is copolymerized with the photo-active dye fluorescein *o*-acrylate (FlA) via surface-initiated reversible addition-fragmentation chain transfer (SI-RAFT) polymerization at varying thicknesses (i.e., molecular weights). The resulting poly(FlA-*co*-NIPAAm) copolymer brushes were found to undergo a rapid structural change between 24 and 26°C, which significantly alters the photocatalytic behavior of the incorporated fluorescein. A wastewater treatment application was implemented to study the effect between temperature and film thickness. Notably, increasing the reaction temperature above the lower critical solution temperature (LCST) increased the performance in the degradation of tetracycline hydrochloride (TC) with the thickest of the photocatalyst polymer brushes showing the most pronounced temperature response.

Introduction

Increasing human population and global water shortage steadily augment the demand for continuous freshwater supply and wastewater remediation.[1–3] Amongst man-made water contaminants are pharmaceuticals, cosmetics, and personal care products, which are discarded into the natural environment during their manufacturing, after their use, or upon disposal.[4–8] Growing evidence regarding their deleterious effects on human health and the environment spawn increasing efforts for alternative and efficient wastewater treatment approaches.[5,9–12] Solutions include membranes, advanced oxidation processes, precipitation, adsorption, or the conventional activated sludge treatment.[13–16]

Photocatalysis has been explored as a viable option to leverage ultraviolet (UV) or visible light – as naturally abundant from the sun – to drive degradation of toxic chemicals and pharmaceuticals into harmless, small substances.[16–19] Examples include the degradation of textile dyes, such as Rhodamine B and Methylene Blue, petroleum hydrocarbons, phenolic compounds, or the removal of heavy metal ions, antibiotics, pesticides, and other contaminants.[14]

While potent, transition metal and organic photocatalysts bear significant limitations that hinder their widespread adoption in wastewater treatment. Amongst these are (i) their expensive nature, (ii) limited solubility in aqueous media due to their aromatic skeletons, and (iii) challenges in their separation from the treated water.[20] These constraints have motivated research into heterogeneous photocatalysts, which has become the most broadly studied method to leverage photocatalysts in wastewater treatment.[13,14,16,17,20,21] For example, metal oxides (e.g. TiO_2 or ZnO) composite photocatalysts have been extensively studied as in the removal of pollutants.[22–30] These heterogeneous photocatalysts require high energy in the ultraviolet region to overcome a large band gap or complex synthetic route to increase their stability.[21] In addition, such metal-based photocatalysts can contaminate the water treatment process, depending on their retrieval and separation method as well as corrode in an aqueous environment.[31,32] Alternative approaches include nanoparticles,[22] polymer networks,[33] or metal organic frameworks[24] (MOFs), which lead

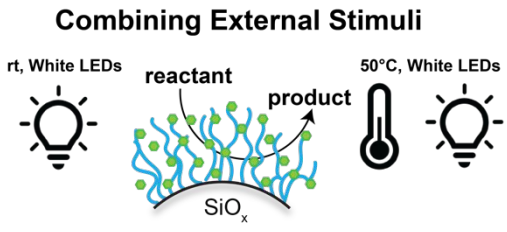

Figure 1. Illustration of the overall idea of combining both thermal and light responsive features on a surface.

[a] *Department of Chemical Engineering, The Pennsylvania State University, University Park, PA 16802, USA.*
[b] *Department of Materials Science and Engineering, The Pennsylvania State University, University Park, PA 16802, USA.*
[c] *Department of Chemistry, The Pennsylvania State University, University Park, PA 16802, USA.*
Electronic Supplementary Information (ESI) available. See DOI: 10.1039/x0xx00000x

to complex separation and recovery steps and decrease recyclability efficiency.

Multi-responsive photoactive polymers are an intriguing and effective approach towards photocatalysis.[20,34,35] Such systems provide tunable photocatalytic activity in response to a second stimulus – e.g., pH,[36] addition of CO_2,[37] or temperature[38] – which expands and/or contracts the catalyst-surrounding matrix or modifies its chemical environment. Proof-of-concept studies exist on how the activity of a network-incorporated photocatalyst can be modulated by modifying steric access to the active sites through external stimuli.[33,39–44] Despite their promise, only a few limited examples of multi-responsive organic heterocatalytic photoactive materials exist.[43,45] Their limitations include inadequate solubility[46,47] or limited synthetic versatility. For polymer-based photocatalysts, separating a synthetic product the photocatalytic polymer often remains prohibitively challenging.

Here, we attempt to address these limitations by engineering a dual responsive heterogeneous photocatalyst (temperature and light) based on photocatalytic polymer brushes (**Figure 1**) that provides tunable photocatalytic properties while allowing facile separation from the reaction mixture. In detail, *N*-isopropylacrylamide (NIPAAm) is copolymerized with the photoactive fluorescein *o*-acrylate (FlA) to produce a multi-responsive smart material poly(FlA-*co*-NIPAAm) (**Figure 2a**). Poly(*N*-isopropylacrylamide) (PNIPAAm) homopolymers are well-known to undergo a change from intramolecular (hydrophillic) to intermolecular (hydrophobic) interactions in H_2O at a lower critical solution temperature ($T_{LCST,avg}$ = 32°C). The LCST of poly(NIPAAm) and its copolymers has been shown to vary based on molecular weight, concentration, composition, and various other parameters.[48] This was leveraged previously to produce thermoresponsive materials, coatings, and surface-tethered macromolecules (polymer brushes) that show well-controlled temperature response.[49–54] PNIPAAm is commonly studied in biomedical applications[48,55–58] or membrane filtration,[59,60] but there has also been interest in its use for wastewater treatment.[61] The described approach provides facile functionalization of inexpensive and optically transparent materials (glass beads) and the ability to tune photocatalytic activity via temperature. The resulting heterogeneous photocatalysts can easily be filtered off and separated from the reaction medium. A model degradation of tetracycline hydrochloride (TC) is studied to highlight utility of these materials in wastewater remediation and examine their dual reactivity. TC is a is a common antibiotic pollutant in aqueous systems.[62,63] While other groups have shown PNIPAAm/photocatalyst systems that generally decrease their activity upon heating, our studies surprisingly show increasing TC degradation at elevated temperatures above the material's LCST.

Results and Discussion

Synthesis of dual responsive substrates

The synthesis of dual responsive polymer brush photocatalytic materials was performed following our previously published surface-initiated reversible addition-fragmentation chain transfer (SI-RAFT) polymerization approach (see Experimental and Supporting Information).[64,65] The RAFT chain transfer agent (CTA) 4-cyano-4-[(dodecylsulfanylthiocarbonyl)sulfanyl] pentanoic acid (CDTPA) was immobilized on soda lime silica (SiO_x) glass beads (D_z = 76.3 μm) to afford SI-RAFT of a thermoresponsive copolymer comprised of 10 mol % fluorescein *o*-acrylate (FlA) in *N*-isopropylacrylamide (NIPAAm) (see **Figure 2a**). All SI-RAFT

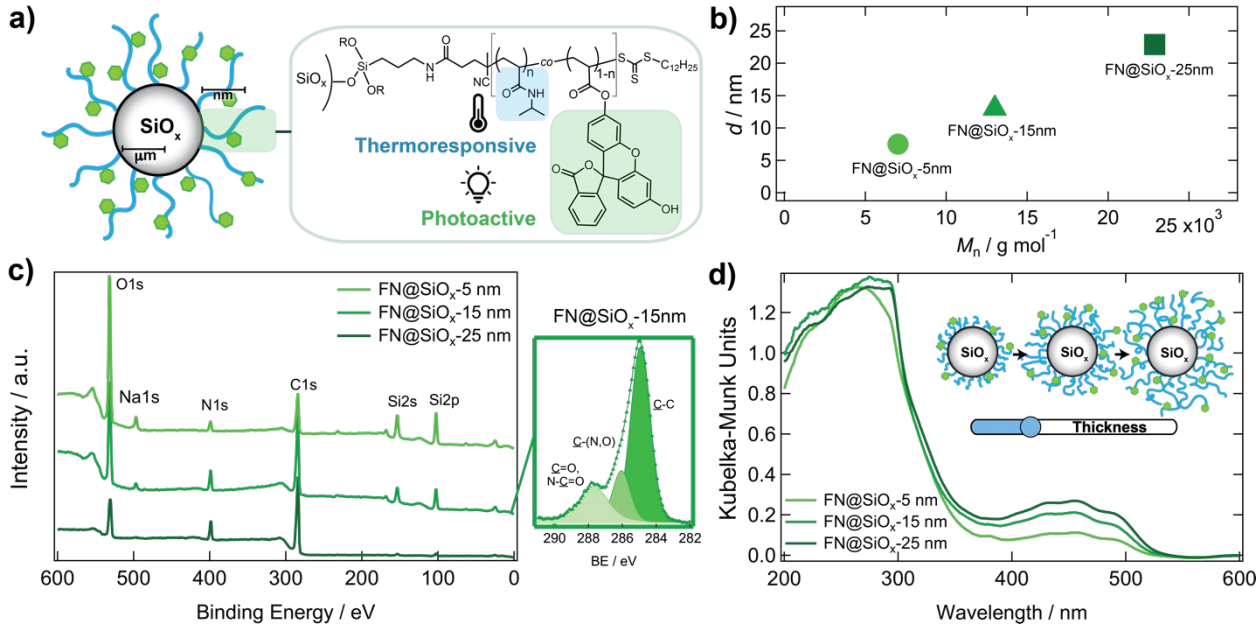

Figure 2. (a) Illustration of the dual-responsive poly(fluorescein *o*-acrylate-*co*-*N*-isopropylacrylamide) heterogeneous catalysts and (b) comparing the experimental molecular weights from the free polymer formed in solution to increasing the thickness of poly(FlA-*co*-NIPAAm) on silicon wafers. Note, the cartoon is not drawn to scale as the polymer brushes are on the nanoscale. The cartoon is not drawn to size. Surface functionalization of FN@SiO_x confirmed through (c) X-ray photoelectron spectroscopy and an example high resolution carbon C1s spectrum for FN@SiO_x-15 nm coating, and (d) ultraviolet-visible diffuse reflectance (UV/vis DR) spectroscopy for the varying thicknesses.

polymerizations were conducted in *N,N*-dimethylformamide (DMF) and initiated via 2,2'-azobis(isobutyronitrile) (AIBN).

Table 1 summarizes the synthesized photocatalytic materials. Poly(FlA-*co*-NIPAAm) polymer brushes (abbreviated as FN@SiO_x) were synthesized at varying monomer to free CTA ratios to control the final polymer brush thickness on the SiO_x surface. Free poly(FlA-*co*-NIPAAm) polymer simultaneously formed in solution were used to determine molecular weight (M_n) and composition via nuclear magnetic resonance spectroscopy (^{1}H NMR, **Table 1**, and **Figure S2-4**). Varying the molar ratio of NIPAAm to CDTPA allowed control over molecular weights. Good agreement was observed between the targeted and experimentally determined incorporation of FlA at an average of 11.7 mol % as determined by ^{1}H NMR (see **Figure S2**). At a feed ratio of 10 mol % in the polymerization mixture, fluorescein incorporation into the copolymer was slightly higher (13 mol %) at lower target molecular weights and decreased incorporation (just under at 9 mol %) at higher NIPAAm:CDTPA ratios. This can be attributed to mass transfer limitations observed by gelation of the reaction mixture at increasing target polymer molecular weights.

Table 1. Summary of the varying film thicknesses and their respective water contact angle (WCA) for the dual responsive polymer brushes.

Entry	Experimental Conditions[a] [NIPAAm]:[FlA]:[CDTPA]	Thickness[b] (*d*, nm)	Water Contact Angle (θ, °)[c]	M_n (g mol^{-1})[d]	FlA Incorporation
1 FN@SiO_x-5	[250]:[25]:[1]	7.5 ± 0.03	65.2 ± 2.8	7,000	13%
2 FN@SiO_x-15	[500]:[50]:[1]	13.1 ± 0.4	65.8 ± 1.2	13,000	13%
3 FN@SiO_x-25	[1000]:[100]:[1]	22.9 ± 0.5	64.8 ± 1.1	22,900	9%
4[e] PNIPAAm	[1000]:[0]:[1]	24.3 ± 1.8	55.6 ± 0.6	16,700	-
5 PFlA	[0]:[100]:[1]	10.8 ± 1.2	46.6 ± 3.4	12,700	100%

[a]NIPAAm = *N*-isopropylacrylamide, FlA = fluorescein *o*-acrylate, CDTPA = 4-cyano-4-[(dodecylsulfanylthiocarbonyl)sulfanyl] pentanoic acid. The thermal SI RAFT polymerization was carried out in inert atmosphere with ABIN (0.25 molar ratio) as initiator at 75°C for 24 hours in DMF. The wafers were cleaned with DCM and MeOH, followed by a stream of nitrogen. [b]Thickness determined through J.A. Woollam RC2-D VASE. [c]WCA measurements determined via an in-house setup (Figure S8). [d]Molecular weight determined through chain-end analysis using ^{1}H NMR in DMSO-d_6. [e]Pure PNIPAAm polymer brush wafer cleaned only with MeOH and molecular weight determined through chain end analysis using ^{1}H NMR

Characterization of the dual responsive surfaces

To estimate thicknesses of the photocatalytic polymer brushes, SI-RAFT was performed simultaneously on both SiO_x glass beads and planar substrates. Variable angle spectroscopic ellipsometry (VASE) was used to quantify the resulting FN@SiO_x polymer brush thickness, *d*, for various [monomer]:[CTA] ratios (see **Table 1**). An average film of $d \approx 7.5$ nm thickness was observed for molar ratio of [NIPAAm]:[FlA]:[CDTPA] of [250]:[25]:[1] (FN@SiO_x-5 nm). Increasing the overall concentration of monomers resulted in an increased brush thickness of $d \approx 22.9 \pm 0.5$ nm ([1000]:[100]:[1] or FN@SiO_x-25 nm). **Figure 2b** shows how the increase of FN@SiO_x film thickness correlated with increasing molecular weights of the poly(FlA-*co*-NIPAAm) copolymers formed in solution (**Figure 2b**).

The resulting FN@SiO_x glass beads and flat silicon wafers were characterized with X-ray photoelectron spectroscopy (XPS). **Figures 2c** and **Figure S5-6** show survey and high-resolution scans of the C1s carbon environment for FN@SiO_x catalysts of varying thicknesses. Increasing polymer brush thickness was evidenced for both glass beads and silicon wafers through the decreasing intensity of the Si2p silicon peak at BE = 102 eV (see survey spectra). In the case of the soda-lime beads, the Na KLL Auger peak at BE = 497 eV decreased with increasing copolymer brush film thickness. High resolution C1s curve fits further verified individual carbon environments on all substrates: C-C (285 eV), C-(N,O) (286.4 eV), and both carbonyl C=O and amide N-C=O carbon atoms (288.0 eV). The nitrogen/carbon signal ratio (N1s:C1s) was used to elucidate the fluorescein *o*-acrylate incorporation. N1s:C1s ratios for the functionalized FN@SiO_x beads were experimentally determined to 0.13, 0.13, and 0.12 for films of 5 nm, 15 nm, and 25 nm targeted thickness, respectively. This matches well with the anticipated ratio of N1s:C1s = 0.12 that was calculated based on a 10 mol % feed of fluorescein *o*-acrylate monomer (**Table S2**). In addition, the similar nitrogen to carbon ratios confirmed the random copolymerization between the NIPAAm and FlA monomers.

The photoactive FN@SiO_x films produced hydrophilic coatings (at room temperature) as apparent from their water contact angles (θ, **Figure S9** and **Table 1**). The CDTPA initiating monolayer exhibited hydrophobic properties ($\theta \approx 94.9 \pm 2.4$

°) prior to SI-RAFT polymerization. In comparison to pure PNIPAAm coatings ($\theta \approx 55.6 \pm 0.6^{\circ}$) and a PFIA films ($\theta \approx 46.6 \pm 3.4^{\circ}$) the copolymerized FN@$SiO_x$ polymer brushes exhibited a slightly increased hydrophobicity at $\theta \approx 65.2 \pm 0.5$ °. Notably, there was no appreciable water contact angle difference between the distinct film thicknesses.

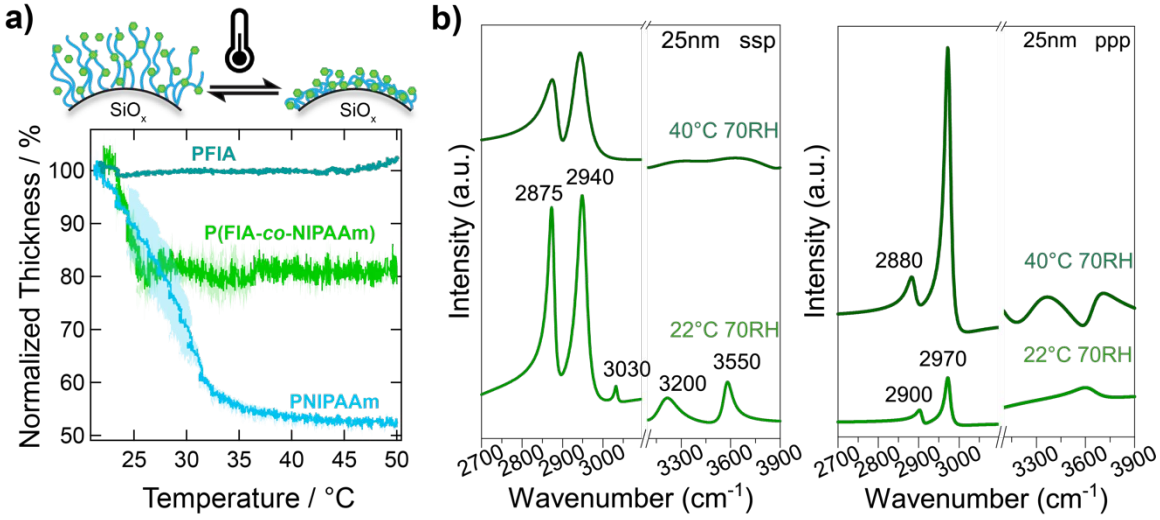

Figure 3. (a) Determination of the lower critical solution temperature (LCST) for the dual-responsive poly(fluorescein *o*-acrylate-*co*-*N*-isopropylacrylamide) polymer brushes compared to only PNIPAAm and PFIA films in deionized water (DIW). (b) Sum frequency generation (SFG) spectra of the FN@SiO_x-25 nm film at 22°C and 40°C in air with 70% relative humidity.

Further, **Figure 2d** shows how the overall concentration of fluorescein increases with FN@SiO_x polymer brush film thickness as determined via ultraviolet-visible (UV/vis) diffuse reflectance (DR) spectroscopy. An emission spectrum was collected via multiphoton microscopy of FN@SiO_x in H_2O (**Figure S7**) to determine the fluorescence of the photocatalyst when polymerized on a surface. When excited, the beads emitted fluorescence at λ_{max} = 500 nm and an observed lifetime of 3.3 ns, which is comparable to reports on fluorescein as a small molecule in solution.[66] Consequently, copolymerizing fluorescein into a surface-tethered polymer appears to not significantly influence its photophysical properties.

Thermoresponsive transition

The thermoresponsive behavior of the FN@SiO_x photocatalytic polymer brush films in deionized water (DIW) was confirmed by monitoring, in situ, the film thickness as a fuction of solution with VASE and a heated liquid cell. **Figure 3a** shows how the FN@SiO_x-15 nm copolymer brush film thickness begins to decrease around 24°C and plateaus above 26°C, yielding a change of ~25% in film thickness (from d_0 = 14.1 nm to d = 10.6 nm). The pure PNIPAAm polymer brush (d_0 = 24.1 nm) displayed a change in thickness over a temperature range from 26°C to 32°C to a final thickness of d = 12.1 nm (**Figure 3a**). As such, the addition of a hydrophobic fluorescein comonomer decreases the LCST from 28°C to 25°C. These findings agree with those of previous groups, where indeed the LCST of a PNIPAAm thin films and polymer brushes were found to be lower than in solution.[53,54] In contrast, the PFIA film control experiment did not show any temperature response and polymer brush thickness remained constant over the examined temperature range (**Figure 3a**).

Vibrational sum frequency generation (SFG) spectroscopic analysis of the FN@SiO_x films showed that the polymer brush surface undergoes substantial changes (**Figure 3b** and **Figure S10**). The ratio of the 2878 cm^{-1} peak in the *ssp* polarization spectrum to the 2970 cm^{-1} peak in the *ppp* polarization spectrum is ~3.4 below LCST and becomes ~0.22 above LCST. This implies that CH_3 groups at the brush end are tilted about 35° from the surface normal when the brush is extended below LCST and reoriented nearly parallel to the surface when the brush is collapsed above LCST.[67] Also, the -N(H)- and -OH groups appear to be nearly normal to the surface below LCST (strong in the *ssp* spectrum) and become more parallel to the surface above LCST (stronger in the *ppp* spectrum).

Degradation of Tetracycline Hydrochloride (TC)

The efficacy of dual responsive FN@SiO_x heterogeneous photocatalysts was evaluated by studying the light-mediated degradation of tetracycline hydrochloride (TC, see **Figure 4b** inset for compound structure). TC is a commonly used antibiotic to treat acne and has been frequently detected in water resources.[62,63] TC is known to cause allergic reactions, exhibit non-specific toxicity in water, and, as an antibiotic, consistent prolonged exposure to TC can lead to the development of resistance and decreased efficiency in patients.[11,62,63]

Figure 4a shows FN@SiO_x-catalyzed TC degradation kinetics for the three distinct FN@SiO_x polymer brush catalysts synthesized. UV/Vis spectroscopy was used to measure how [TC] concentration changes with time (C/C_0, see **Figure 4b** for an example of raw UV/vis data). Experiments were performed by irradiating a solution of TC in deionized water (DIW) with white LEDs (**Figure S11** and **Figure S17** for irradiation of natural sunlight). To interrogate the influence of temperature, experiments were performed below LCST (T = 22°C) and at elevated temperature above LCST (T = 50°C, **Figure S11**). Before any data collection, the molar absorptivity coefficient was

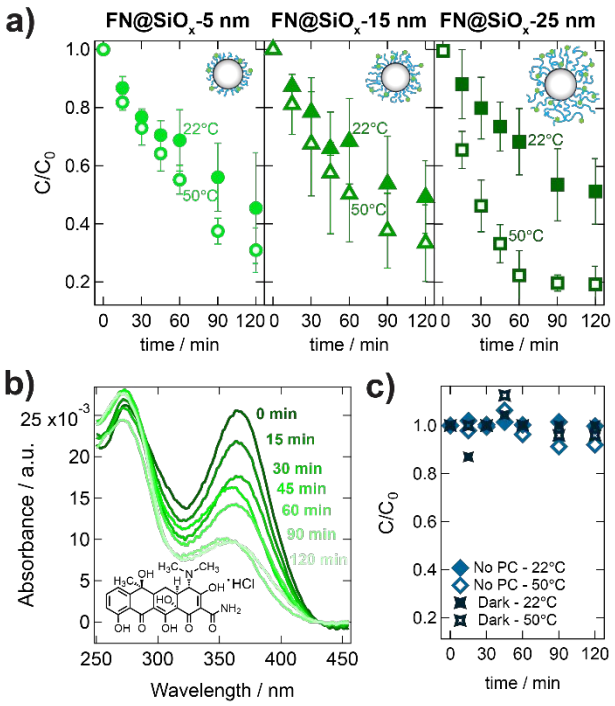

Figure 4. (a) Photocatalytic degradation of tetracycline hydrochloride (TC) kinetic performance of the different FN@SiO_x heterogeneous dual-responsive catalysts at a temperature above and below the LCST. (b) Example raw UV/vis data for the degradation of TC with FN@SiO_x-15 nm at room temperature with an inset of TC's molecular structure. (c) Control experiments attempting degradation of TC in the dark and absence of photocatalyst.

determined via a calibration curve of TC at varying concentrations (ε = 1.62 × 10^7 M^{-1} cm^{-1} at λ = 356 nm, **Figure S12**).

At room temperature (T < LCST), little difference in degradation rates was observed between the photocatalytic brushes of different thicknesses (**Figure 4a**). We found this surprising, considering that UV/vis DR spectroscopy (see **Figure 2d**) clearly indicated an increased fluorescein concentration with the brush thickness. Approximately 50% of the TC is degraded after 2 hours of reaction time, corresponding to an average 0.0065 min^{-1} rate constant (k) as determined by a pseudo-first order reaction rate from ln(C/C_0) with respect to time (t, **Figure S13** and **Table S4**).

$$\ln\left(\frac{C}{C_0}\right) = kt \qquad (1)$$

In contrast, elevating the temperature to 50°C, i.e., above T > LCST, improves degradation rates for all catalysts (see **Figure S13** and **Table S4** for summary of rate constants). Notably, thicker poly(FlA-*co*-NIPAAm) brushes lead to faster TC degradation rates (**Figure 4** and **S13**). The catalytic efficiency increases from ~50% to ~68% for both FN@SiO_x-5 nm and FN@SiO_x-15 nm with an average of 0.0102 min^{-1} rate constant. Interestingly, the thickest brush (FN@SiO_x-25 nm) demonstrates the most response to temperature – while at room temperature it does not significantly stand out when compared to thinner photocatalytic films. For FN@SiO_x-25 nm, the degradation of TC almost doubled in efficiency increasing from from 49% (RT) to 81% (50°C), with an increased 0.0175 min^{-1} rate constant. This suggests a conformational rearrangement of the polymer brushes above LCST (**Figure 3b and Figure S10**), which would affect the availability of fluorescein for photocatalysis either by being exposed at the outermost surface or the chain end conformations allowing more ingress of TC into the brush.

Control experiments in the absence of photocatalysts (but under irradiation) or in the dark showed no significant degradation of the TC antibiotics and negligible temperature effects or thermal degradation were observed (see **Figure 4c** and **Figure S14**).

Based on these findings, the dual thermo- and photo-active heterogeneous catalysts show improved performance at elevated temperatures. We hypothesize that the conformational collapse of the PNIPAAm backbone above LCST leads to an increased accessibility of TC to the fluorescein photocatalysts. This would improve catalytic performance for all films but be most pronounced for thicker films. As such, this hypothesis aligns well with our experimental findings.

Notably, this result contrasts with previous work on thermoresponsive photocatalysis.[68–71] For example, Huo et al. used PNIPAM@AgBr/CSs nanocomposites for the degradation of tetracyline for a dual-responsive purpose. They found that above the LCST and higher temperatures, the degradation rate decreased.[72] In another multi-responsive study, Yoon et al. observed with a hybrid Au-PNIPAM film with ZnO nanoparticles, an increase in performance at elevated temperatures in the degradation of *p*-nitrophenol for thin films and low molecular weights.[73] However, at high molecular weights and thicker films they noticed a decrease in catalyst efficiency at a temperature above the LCST.[73] Initially, their studies are in agreement with our findings at FN@SiO_x-5,15 nm; however, the higher molecular weight and thicker films are contrasting our investigation with a fully organic dual responsive heterogeneous catalyst.

Preliminary studies show similar results for other compounds in water remediation efforts. For the removal of the dye methylene blue (MB), FN@SiO_x-25 nm degraded 79% of MB at room temperature (**Figure 18b**). The catalytic efficiency increased to 97% at elevated temperatures, which is complementary to what we are observing in the degradation of TC. Further studies are going towards the study of other substrates and whether this is a universal trend for different compounds.

We further tested the stability of the FN@SiO_x substrates by recycling them in three consecutive degradations of TC at the two different temperatures (**Figure S16**). Recovery through simple filtration successfully allowed the reusability of FN@SiO_x-25 nm beads with negligible difference in catalytic performance over each reaction cycle. While Mao et al. recycled their dual responsive nanoparticles (ZnPC-*g*-TiO_2-*g*-PNIPAAm) in the removal of the dye Rhodamine B (RhoB) at room temperature for three cycles, their separation process included a high-speed centrifugation and elevated temperatures of 45°C.[69] The size of our supports eliminates the time and effort

it takes to recovery the heterogeneous catalysts typically needed for such processes, increasing recyclability efficiency.

Conclusions

We described the synthesis of a dual-responsive heterogeneous catalyst based on photocatalytic polymer brushes comprised of thermoresponsive *N*-isopropylacrylamide (NIPAAm) and photoactive fluorescein *o*-acrylate (FlA). The resulting surface-tethered photoactive poly(FlA-*co*-NIPAAm) polymer brushes showed well-controlled temperature response in water, in agreement with LCST behavior. To highlight the utility of these materials in wastewater remediation, we examined their dual reactivity for a model degradation of tetracycline hydrochloride (TC). At room temperature (T < LCST), little difference in degradation rates was observed between the photocatalytic brushes of different thicknesses. At T > LCST, degradation rates are improved for all catalysts and thicker poly(FlA-*co*-NIPAAm) brushes lead to higher TC degradation rates. Interestingly, the thickest brush demonstrated the most pronounced temperature response, while it does not significantly stand out when compared to thinner photocatalytic films at room temperature.

Author Contributions

All authors approved the final version of the manuscript.

Corresponding Author

*pester@psu.edu

Acknowledgements

C.W.P. acknowledges the National Science Foundation (NSF CBET Award # 2143628) for financial support. The authors would like to thank Dr. T. J. Zimudzi (PSU Materials Characterization Lab) for assistance with obtaining UV/vis data, Winters Guo and Prof. Gina Noh for UV/vis DR support, and Prof. Bryan Vogt and Minseo Kim for support with ellipsometry data collection and fitting. In addition, the authors would like to acknowledge Axalta for supporting the SFG data collection.

Funding sources

National Science Foundation (NSF CBET Award # 2143628).

References

1. Eliasson, J. *Nature*, 2015, **517**.
2. Cohen, J. E. *Science (1979)*, 2003, **302**, 1172–1175.
3. Bigas, H. Water security and the global water agenda : a UN-water analytical brief, United Nations University - Institute for Water, Environment and Health, 2013.
4. Unesco, World Water Assessment Programme (United Nations), UN-Water Water and climate change, .
5. Wilkinson, J. L., Boxall, A. B. A., Kolpin, D. W., Leung, K. M. Y., Lai, R. W. S., Galban-Malagon, C., Adell, A. D., Mondon, J., Metian, M., Marchant, R. A., Bouzas-Monroy, A., Cuni-Sanchez, A., Coors, A., Carriquiriborde, P., Rojo, M., Gordon, C., Cara, M., Moermond, M., Luarte, T., Petrosyan, V., Perikhanyan, Y., Mahon, C. S., McGurk, C. J., Hofmann, T., Kormoker, T., Iniguez, V., Guzman-Otazo, J., Tavares, J. L., Gildasio De Figueiredo, F., Razzolini, M. T. P., Dougnon, V., Gbaguidi, G., Traore, O., Blais, J. M., Kimpe, L. E., Wong, M., Wong, D., Ntchantcho, R., Pizarro, J., Ying, G.-G., Chen, C.-E., Paez, M., Martinez-Lara, J., Otamonga, J.-P., Pote, J., Ifo, S. A., Wilson, P., Echeverria-Saenz, S., Udikovic-Kolic, N., Milakovic, M., Fatta-Kassinos, D., Ioannou-Ttofa, L., Belusova, V., Vymazal, J., Cardenas-Bustamante, M., Kassa, B. A., Garric, J., Chaumot, A., Gibba, P., Kunchulia, I., Seidensticker, S., Lyberatos, G., Halldorsson, H. P., Melling, M., Shashidhar, T., Lamba, M., Nastiti, A., Supriatin, A., Pourang, N., Abedini, A., Abdullah, O., Gharbia, S. S., Pilla, F., Chefetz, B., Topaz, T., Yao, K. M., Aubakirova, B., Beisenova, R., Olaka, L., Mulu, J. K., Chatanga, P., Ntuli, V., Blama, N. T., Sherif, S., Aris, A. Z., Looi, L. J., Niang, M., Traore, S. T., Oldenkamp, R., Ogunbanwo, O., Ashfaq, M., Iqbal, M., Abdeen, Z., O'Dea, A., Morales-Saldana, J. M., Custodio, M., de la Cruz, H., Navarrete, I., Carvalho, F., Gogra, A. B., Koroma, B. M., Cerkvenik-Flajs, V., Gombac, M., Thwala, M., Choi, K., Kang, H., Ladu, J. L. C., Rico, A., Amerasinghe, P., Sobek, A., Horlitz, G., Zenker, A. K., King, A. C., Jiang, J.-J., Kariuki, R., Tumbo, M., Tezel, U., Onay, T. T., Lejju, J. B., Vystavna, Y., Vergeles, Y., Heinzen, H., Perez-Parada, A., Sims, D. B., Figy, M., Good, D., Teta, C. *PNAS*, 2022.
6. aus der Beek, T., Weber, F. A., Bergmann, A., Hickmann, S., Ebert, I., Hein, A., Küster, A. *Environ Toxicol Chem*, 2016, **35**, 823–835.
7. Kolpin, D. W., Furlong, E. T., Meyer, M. T., Thurman, E. M., Zaugg, S. D., Barber, L. B., Buxton, H. T. *Environ Sci Technol*, 2002, **36**, 1202–1211.
8. Boxall, A. B. A., Rudd, M. A., Brooks, B. W., Caldwell, D. J., Choi, K., Hickmann, S., Innes, E., Ostapyk, K., Staveley, J. P., Verslycke, T., Ankley, G. T., Beazley, K. F., Belanger, S. E., Berninger, J. P., Carriquiriborde, P., Coors, A., DeLeo, P. C., Dyer, S. D., Ericson, J. F., Gagné, F., Giesy, J. P., Gouin, T., Hallstrom, L., Karlsson, M. v., Joakim Larsson, D. G., Lazorchak, J. M., Mastrocco, F., McLaughlin, A., McMaster, M. E., Meyerhoff, R. D., Moore, R., Parrott, J. L., Snape, J. R., Murray-Smith, R., Servos, M. R., Sibley, P. K., Straub, J. O., Szabo, N. D., Topp, E., Tetreault, G. R., Trudeau, V. L., van der Kraak, G. *Environ Health Perspect*, 2012, 120, 1221–1229.
9. Gkika, D. A., Mitropoulos, A. C., Lambropoulou, D. A., Kalavrouziotis, I. K., Kyzas, G. Z. *Environmental Science and Pollution Research*, 2022, 29, 75223–75247.
10. Kidd, K. A., Blanchfield, P. J., Mills, K. H., Palace, V. P.,

Evans, R. E., Lazorchak, J. M., Flick, R. W. *PNAS*, 2017, **104**, 8897–8901.
11. Wellington, E. M. H., Boxall, A. B. A., Cross, P., Feil, E. J., Gaze, W. H., Hawkey, P. M., Johnson-Rollings, A. S., Jones, D. L., Lee, N. M., Otten, W., Thomas, C. M., Williams, A. P. *Lancet Infect Dis*, 2013, **12**, 155–165.
12. Brodin, T., Fick, J., Jonsson, M., Klaminder, J. *Science (1979)*, 2013, **339**, 814–815.
13. Miklos, D. B., Remy, C., Jekel, M., Linden, K. G., Drewes, J. E., Hübner, U. *Water Res*, 2018, 139, 118–131.
14. Ren, G., Han, H., Wang, Y., Liu, S., Zhao, J., Meng, X., Li, Z. *Nanomaterials*, 2021, 11.
15. Grandclément, C., Seyssiecq, I., Piram, A., Wong-Wah-Chung, P., Vanot, G., Tiliacos, N., Roche, N., Doumenq, P. *Water Res*, 2017, 111, 297–317.
16. Rueda-Marquez, J. J., Levchuk, I., Fernández Ibañez, P., Sillanpää, M. *J Clean Prod*, 2020, 258, 1–13.
17. Šuligoj, A., Cerc Korošec, R., Žerjav, G., Novak Tušar, N., Lavrenčič Štangar, U. *Top Curr Chem*, 2022, 380.
18. Shokri, A., Sanavi Fard, M. *Chemical Papers*, 2022, 76, 5309–5339.
19. Ahmed, S. N., Haider, W. *Nanotechnology*, 2018, 29.
20. Li, R., Landfester, K., Ferguson, C. T. J. *Angewandte Chemie - International Edition*, 2022.
21. Nguyen, T. D., Lee, T., Van Tran, T., Nguyen, V. H., Nong, L. X., Bach, L. G., Vo, D. V. N. *Environ Chem Lett*, 2022.
22. Alhokbany, N., Ahamad, T., Alshehri, S. M. *J Environ Chem Eng*, 2022, **10**.
23. Chen, C. R., Zeng, H. Y., Yi, M. Y., Xiao, G. F., Zhu, R. L., Cao, X. J., Shen, S. G., Peng, J. W. *Ecotoxicol Environ Saf*, 2019, **172**, 423–431.
24. Kaur, M., Mehta, S. K., Kansal, S. K. *Environmental Science and Pollution Research*, 2022.
25. Li, W., Chu, X. S., He, S. A., Wang, X. C., Wang, C. Y. *Environ Sci Nano*, 2020, **7**, 2654–2668.
26. Ren, Y. N., Xu, W., Zhou, L. X., Zheng, Y. Q. *Polyhedron*, 2018, **139**, 63–72.
27. Ren, Y. N., Xu, W., Si, Z. X., Zhou, L. X., Zheng, Y. Q. *Polyhedron*, 2018, **152**, 195–201.
28. Shen, J. C., Zeng, H. Y., Chen, C. R., Xu, S. *Appl Clay Sci*, 2020, **185**.
29. Wang, W., Fang, J., Shao, S., Lai, M., Lu, C. *Appl Catal B*, 2017, **217**, 57–64.
30. Yang, H., Yang, J. *RSC Adv*, 2018, **8**, 11921–11929.
31. Weng, B., Qi, M. Y., Han, C., Tang, Z. R., Xu, Y. J. *ACS Catal*, 2019, 9, 4642–4687.
32. Mashuri, S. I. S., Ibrahim, M. L., Kasim, M. F., Mastuli, M. S., Rashid, U., Abdullah, A. H., Islam, A., Asikin-Mijan, N., Tan, Y. H., Mansir, N., Kaus, N. H. M., Hin, T. Y. Y. *Catalysts*, 2020, 10, 1–29.
33. Amir, F., Li, X., Gruschka, M. C., Colley, N. D., Li, L., Li, R., Linder, H. R., Sell, S. A., Barnes, J. C. *Chem Sci*, 2020, **11**, 10910–10920.
34. Urban, A. M., Urban, M. W. M. Urban, Ed.; ACS Symposium Series 2005;
35. Jochum, F. D., Theato, P. *Chem Soc Rev*, 2013, **42**, 7468–7483.
36. Chen, M., Deng, S., Gu, Y., Lin, J., MacLeod, M. J., Johnson, J. A. *J Am Chem Soc*, 2017, **139**, 2257–2266.
37. Byun, J., Huang, W., Wang, D., Li, R., Zhang, K. A. I. *Angewandte Chemie International Edition*, 2018, **57**, 2967–2971.
38. De, P., Li, M., Gondi, S. R., Sumerlin, B. S. *J Am Chem Soc*, 2008, **130**, 11288–11289.
39. Ferguson, C. T. J., Huber, N., Landfester, K., Zhang, K. A. I. *Angewandte Chemie International Edition*, 2019, **58**, 10567–10571.
40. Chen, J., Liu, M., Huang, H., Deng, F., Mao, L., Wen, Y., Huang, L., Tian, J., Zhang, X., Wei, Y. *J Mol Liq*, 2018, **259**, 179–185.
41. Hernández, P., Lucero-Acuña, A., Gutiérrez-Valenzuela, C. A., Moreno, R., Esquivel, R. *E-Polymers*, 2017, **17**, 399–408.
42. Kamzabek, D., le Dé, B., Coche-Guérente, L., Miomandre, F., Dubacheva, G. v. *Langmuir*, 2021, **37**, 10971–10978.
43. Olson, R. A., Levi, J. S., Scheutz, G. M., Lessard, J. J., Figg, C. A., Kamat, M. N., Basso, K. B., Sumerlin, B. S. *Macromolecules*, 2021, **54**, 4880–4888.
44. Lessard, J. J., Scheutz, G. M., Korpusik, A. B., Olson, R. A., Figg, C. A., Sumerlin, B. S. *Polym Chem*, 2021, **12**, 2205–2209.
45. González-Muñoz, D., Gómez-Avilés, A., Molina, C. B., Bedia, J., Belver, C., Alemán, J., Cabrera, S. *J Mater Sci Technol*, 2022, **103**, 134–143.
46. Woods, D. J., Sprick, R. S., Smith, C. L., Cowan, A. J., Cooper, A. I. *Adv Energy Mater*, 2017, **7**.
47. Stando, K., Kasprzyk, P., Felis, E., Bajkacz, S. *Molecules*, 2021, **26**.
48. Sarwan, T., Kumar, P., Choonara, Y. E., Pillay, V. *Front Mater*, 2020, 7.
49. Furyk, S., Zhang, Y., Ortiz-Acosta, D., Cremer, P. S., Bergbreiter, D. E. *J Polym Sci A Polym Chem*, 2006, **44**, 1492–1501.
50. Jia, X., Jiang, X., Liu, R., Yin, J. *Macromol Chem Phys*, 2009, **210**, 1876–1882.
51. Liang, L., Feng, X., Liu, J., Rieke, P. C. *J Appl Polym Sci*, 1999, **72**, 1–11.
52. Plunkett, K. N., Zhu, X., Moore, J. S., Leckband, D. E. *Langmuir*, 2006, **22**, 4259–4266.
53. Xue, C., Yonet-Tanyeri, N., Brouette, N., Sferrazza, M., Braun, P. V., Leckband, D. E. *Langmuir*, 2011, **27**, 8810–8818.
54. Yu, Y., Kieviet, B. D., Liu, F., Siretanu, I., Kutnyánszky, E., Vancso, G. J., De Beer, S. *Soft Matter*, 2015, **11**, 8508–8516.
55. Sponchioni, M., Capasso Palmiero, U., Moscatelli, D. *Materials Science and Engineering C*, 2019, 102, 589–605.
56. Kim, Y. J., Matsunaga, Y. T. *J Mater Chem B*, 2017, 5, 4307–4321.

57. Pietsch, C., Schubert, U. S., Hoogenboom, R. *Chemical Communications*, 2011, **47**, 8750–8765.
58. Ward, M. A., Georgiou, T. K. *Polymers (Basel)*, 2011, **3**, 1215–1242.
59. Ng, W. S., Connal, L. A., Forbes, E., Franks, G. V. *Miner Eng*, 2018, **123**, 144–159.
60. Xu, D., Zheng, J., Zhang, X., Lin, D., Gao, Q., Luo, X., Zhu, X., Li, G., Liang, H., Van der Bruggen, B. *Environ Sci Technol*, 2022, **56**, 1927–1937.
61. Xu, X., Bizmark, N., Christie, K. S. S., Datta, S. S., Ren, Z. J., Priestley, R. D. *Macromolecules*, 2022, 55, 1894–1909.
62. Javid, A., Mesdaghinia, A., Nasseri, S., Mahvi, A. H., Alimohammadi, M., Gharibi, H. *J Environ Health Sci Eng*, 2016, **14**.
63. Hoa, P. T. P., Managaki, S., Nakada, N., Takada, H., Shimizu, A., Anh, D. H., Viet, P. H., Suzuki, S. *Science of the Total Environment*, 2011, **409**, 2894–2901.
64. Bell, K., Freeburne, S., Wolford, A., Pester, C. W. *Polym Chem*, 2022.
65. Bell, K., Freeburne, S., Fromel, M., Oh, H. J., Pester, C. W. *Journal of Polymer Science*, 2021, **59**, 2844–2853.
66. Kristoffersen, A. S., Erga, S. R., Hamre, B., Frette, Ø. *J Fluoresc*, 2018, **28**, 1065–1073.
67. Lin, Y. T., Fromel, M., Guo, Y., Guest, R., Choi, J., Li, Y. S., Kaya, H., Pester, C. W., Kim, S. H. *Langmuir*, 2022, **38**, 14704–14711.
68. Huo, P., Li, J., Ye, Z., Wang, H., Liu, X., Li, X., Yan, Y. *Chinese Chemical Letters*, 2017, **28**, 2259–2262.
69. Mao, B., Liu, C., Cui, X., Li, Y., Duan, Q. *Molecules*, 2022, **27**.
70. Sun, L., Zhou, Y., Li, X., Li, J., Shen, D., Yin, S., Wang, H., Huo, P., Yan, Y. *Chinese Journal of Catalysis*, 2020, **41**, 1573–1588.
71. Yu, Z., Tang, D., Lv, H., Feng, Q., Zhang, Q., Jiang, E., Wang, Q. *Colloids Surf A Physicochem Eng Asp*, 2015, **471**, 117–123.
72. Huo, P., Ye, Z., Wang, H., Guan, Q., Yan, Y. *J Alloys Compd*, 2017, **696**, 701–710.
73. Yoon, M., Lee, J. E., Jang, Y. J., Lim, J. W., Rani, A., Kim, D. H. *ACS Appl Mater Interfaces*, 2015, **7**, 21073–21081.